Journal of Materials Chemistry B

PAPER

View Article Online
View Journal | View Issue

Cite this: J. Mater. Chem. B, 2018, 6, 1633

Induction of oxidative stress and sensitization of cancer cells to paclitaxel by gold nanoparticles with different charge densities and hydrophobicities†

Hainan Sun,[a] Yin Liu,[b] Xue Bai,[a] Xiaofei Zhou,[a] Hongyu Zhou,*[c] Sijin Liu [b] and Bing Yan *[a]

Received 6th December 2017,
Accepted 5th February 2018

DOI: 10.1039/c7tb03153j

rsc.li/materials-b

An elevated reactive oxygen species (ROS) level leads to cellular oxidative stress, which has long been associated with diseases, such as cancer. Thus, the understanding and appropriate manipulation of cellular oxidative stress are needed for disease treatment. It has been reported that nanoparticles induce oxidative stress in human cells through different pathways. However, how the physicochemical properties of nanoparticles perturb cellular oxidative stress remains unclear. In this paper, we explored the effects of the positive/negative charge density and hydrophobicity of gold nanoparticles (GNPs) on the induction of oxidative stress and related mechanisms. In multiple human cell lines, we found that only the positive charge density and hydrophobicity of nanoparticles were correlated with the induction of cellular oxidative stress. Hydrophobic nanoparticles generated oxidative stress mainly through NADPH oxidase activation while positively charged nanoparticles generated it through perturbations of the mitochondria and modulation of intracellular Ca^{2+} concentration. Furthermore, nanoparticle-induced oxidative stress sensitized paclitaxel-induced cancer cell killing by 200%. These findings provided unequivocal structural parameters for the design of future nanomedicine and biocompatible nanocarriers.

1. Introduction

An elevated reactive oxygen species (ROS) level in cells leads to cellular oxidative stress, which is associated with aging,[1] cancer,[2] neurodegeneration,[3] diabetes,[4] and atherosclerosis.[5] For example, Alzheimer's disease is associated with oxidative stress-induced accumulation of amyloid-β peptides.[3] Oxidative stress-induced DNA damage is responsible for tumorigenesis.[6] On the other hand, if the oxidative stress is kept at a high level, cancer cells will undergo apoptotic death. Thus, therapeutic agents that are designed to elicit oxidative stress are promising candidates in disease treatment.[7] Furthermore, the reversal of the intracellular antioxidant capacity by accelerating oxidative stress production may sensitize anti-tumor drugs[8,9] and promote cell cytotoxicity. Therefore, the understanding and appropriate manipulation of cellular oxidative stress are needed for disease treatment and drug development.

Nanotechnology has been widely applied in industry,[10–13] biomedicine,[14–16] and over 1827 consumer products.[17,18] Meanwhile, nanoparticles are now routine pollutants in the environment, such as in air and water. Therefore, nanoparticles may enter the human body through various pathways, such as inhalation, oral exposure, and intravenous injection. Upon entering the human body, nanoparticles may interact with biomolecules through specific and nonspecific interactions and induce oxidative stress in human cells through different pathways.[19] It has been reported that oxidative stress elicited by zinc oxide nanoparticles leads to cytotoxicity.[20] Cerium oxide nanoparticle-induced oxidative stress sensitizes pancreatic cancer cells to radiation.[21] The core materials,[22,23] sizes,[24] shapes[25] and surface chemistries[26–28] of nanoparticles may be crucial factors in inducing cellular oxidative stress and dictation of biocompatibility.[29] For example, ROS induced by graphene oxide (GO) impaired the development of zebrafish embryos.[30] Functionalization of GO with L-cysteine could alleviate the ROS production.[31] However, when the core material (with the same band gap) and the nanoparticle shape are identical, how the physicochemical properties of nanoparticles perturb cellular

[a] School of Chemistry and Chemical Engineering, Shandong University, Jinan 250100, China. E-mail: drbingyan@yahoo.com
[b] State Key Laboratory of Environmental Chemistry and Ecotoxicology, Research Center for Eco-Environmental Sciences, Chinese Academy of Sciences, Beijing 100085, China
[c] School of Environment, Guangzhou Key Laboratory of Environmental Exposure and Health and Guangdong Key Laboratory of Environmental Pollution and Health, Jinan University, Guangzhou 510632, China. E-mail: hyzhou001@gmail.com

† Electronic supplementary information (ESI) available. See DOI: 10.1039/c7tb03153j

oxidative stress remains unclear. Therefore, systematic elucidation of the effect of the physicochemical properties of nanoparticles on the induction of oxidative stress warrants an important study for the further understanding of nano-toxicology and nano-medicine.

In this work, hydrophobicity and positive charge were identified as key factors for gold nanoparticle (GNP)-induced cellular oxidative stress. Mechanisms for these effects were NADPH oxidase activation by hydrophobic nanoparticles and mitochondria perturbation and intracellular Ca^{2+} concentration modulation by positively charged nanoparticles, respectively. A 2-fold enhancement was found in HeLa cells when treated with both GNPs and paclitaxel, demonstrating the sensitization of cancer cells to anti-tumor drugs by accelerating oxidative stress production.

2. Experimental section

2.1. Synthesis of gold nanoparticle (GNP) libraries

Taking the synthesis of the library with a gradient change in hydrophobicity (HY) with a diameter of 6 nm as an example, hydrogen tetrachloroaurate(III) trihydrate solution (1.25 mL, 0.061 mmol) was added to a solution of a hydrophilic/hydrophobic ligand in DMF. For HY 1 to HY 7, the amount of the hydrophilic/hydrophobic ligand was 20.2 mg/0 mg, 18.1 mg/0.8 mg, 16.1 mg/1.6 mg, 9.7 mg/2.6 mg, 6.0 mg/3.2 mg, 4.0 mg/4.9 mg, and 0 mg/8.3 mg, respectively. After stirring for 30 min, sodium tetrahydroborate (10 mg, 0.264 mmol) in water was added dropwise. The solution was stirred overnight. In order to remove the free ligands and DMF, the solution was centrifuged at 15 000 rpm for 20 min. The supernatant was decanted and the solid was dissolved in deionized water and centrifuged again. The wash-centrifugation operation was repeated five times.

2.2. Characterization of the GNP libraries

The transmission electron microscopy (TEM) analysis of the GNPs was performed using a JEM-1011 (Japan) transmission electron microscope. The diameters of the GNPs were measured using Image Pro Plus 6.0. For the analysis of hydrodynamic diameter and zeta potential, the GNPs were diluted in ultrapure water (18.2 MΩ) at 50 μg mL^{-1}, which were measured using a Zetasizer Nano ZS laser particle size analyzer (Malvern Instruments Ltd, Malvern, UK). Ligands on the GNPs were firstly cleaved by I_2 and then were investigated by LC/MS. A modified "shaking flask" method was employed in the measurement of the hydrophobicity of the GNPs as described in our previous article.[28]

2.3. Quantification of the heme oxygenase 1 (HO-1) level

After incubation with the GNPs (50 μg mL^{-1}) for 24 h, A549 cells were washed with PBS 3 times, scraped from the culture vessel using a cell scraper, and subsequently centrifuged at 1500 rpm for 10 min at 4 °C. The supernatant was discarded, and the HO-1 level in the A549 cells was determined by western blot, where β-actin was used as a loading control. The band density was quantified using ImageJ. The HO-1 level was quantified by the ratio of the band densities of HO-1 over β-Actin.

2.4. Intracellular H_2O_2 assay

Intracellular H_2O_2 was assessed using the ROS-Glo™ H_2O_2 assay (G8820, Promega). The cells were cultured in a 96-well plate overnight. The medium was removed and the cells were treated with the GNPs for 22 h before 20 μL of H_2O_2 substrate solution was added to each well. The cells were kept at 37 °C for 2 h. Afterward, a ROS-Glo detection solution (100 μL) was added to each well and incubated for 20 min at room temperature. The luminescence was determined using a microplate reader. H_2O_2 (200 μM) was used as a positive control.

2.5. Mitochondria and NADPH oxidase inhibitors

The A549 cells were pretreated with apocynin (APO, NADPH oxidase inhibitor, 20 μM or 100 μM), diphenyleneiodonium chloride (DPI, NADPH oxidase inhibitor, 1 μM or 5 μM) or rotenone (ROT, mitochondrial respiratory chain complex **1** inhibitor, 0.2 μM or 1 μM) for 30 min prior to incubation with GNPs for 24 h. The intracellular H_2O_2 level was determined by the ROS-Glo™ H_2O_2 assay.

2.6. NADPH oxidase activation

MRC-5, HepG2 and A549 cells that contain NADPH oxidase at various levels were cultured in a cell culture medium in the presence or absence of HY 7 (6 nm, 50 μg mL^{-1}) for 24 h. The $p47^{phox}$ level in the cell membranes was determined by western blot. The band density was quantified using ImageJ. The relative level of $p47^{phox}$ in the cell membranes was defined as the ratio of the band densities of $p47^{phox}$ in the presence of HY 7 over $p47^{phox}$ in the cell culture medium.

2.7. Calcium flux analysis

The A549 cells were treated with GNPs for 24 h at the indicated concentration. The cells were washed with DPBS three times. Afterward, the cells were treated with 10 μM of Fluo-3 AM in a culture medium and kept in the dark at room temperature for 1 h and at 37 °C for 30 min. The cells were washed with DPBS three times. The mean fluorescence intensity was measured using a microplate reader.

2.8. Calcium chelating agent

The A549 cells were pretreated with a Ca^{2+} chelating agent BAPTA-AM (10 μM, or 20 μM) for 30 min prior to incubation with GNPs with the highest positive charge (PO) density PO 6 (6 nm) at a concentration of 50 μg mL^{-1} for 24 h. The intracellular H_2O_2 level was determined by the ROS-Glo™ H_2O_2 assay.

2.9. EC_{50} of paclitaxel (PTX) affected by nanoparticles and *N*-acetyl-L-cysteine (NAC)

HeLa cells were treated with various concentrations of PTX (0.1 nM–10 μM) in the presence or absence of PO 6, HY 7 (50 μg mL^{-1}), and NAC (10 mM) for 24 h. The cells were lysed and analyzed by the CellTilter-Glo® luminescent cell viability assay through luminescence determination using a microplate reader.

3. Results and discussion

3.1. Synthesis and characterization of the GNP libraries of univariant gradient changes in surface charge density and hydrophobicity

To get a better understanding of how the physicochemical properties of nanoparticles perturb cellular oxidative stress, we firstly synthesized three GNP libraries with a diameter of 6 nm and a univariant gradient change of a single physicochemical property (Fig. 1a), such as hydrophobicity (HY), positive charge (PO) density, and negative charge (NE) density, using similar methods to those mentioned in our previous work.[28,32] To obtain GNP libraries of gradient changes in specific physicochemical properties, we chemically modified the nanoparticle surface with two different molecules. For example, by varying the ratio of a neutral and a positively charged molecule, we synthesized a GNP library containing six nanoparticles (PO 1–6) with a gradual change in the PO density. Applying the same principle, we also synthesized GNP libraries with gradual changes in NE and HY. The quantity of ligands on each nanoparticle was measured by LC/MS we developed (Fig. 1b–d).[33] For example, the number of hydrophobic ligands on the GNPs in the HY library ranged from 0 to 727 per particle, while the number of hydrophilic ligands ranged from 459 to 0, indicating a total ligand number between 386 and 727 per particle. From the ratio of the two different ligands (Fig. 1d) and the experimental log *P* values (Fig. S1, ESI†) of each library member, we can clearly see the gradient change of the hydrophobicity. The diameter of the GNPs was approximately 6 nm, as measured by TEM (Fig. S2, ESI†). The hydrodynamic diameters of the GNPs with different surface chemistry in water were approximately 30–100 nm as measured by dynamic light scattering (DLS), indicating the different degrees of aggregation of the GNPs (Fig. S3a, ESI†). The GNPs in PO and NE libraries showed hydrodynamic diameters of around 30 nm, while the GNPs in the HY library showed increased hydrodynamic diameters with the increase of hydrophobicity. As expected, the zeta potential values of most members in the NE and HY libraries were lower than −20 mV, while the GNPs in the PO library had zeta potential values greater than 30 mV expect PO 1 (neutral nanoparticle), indicating different electrostatic properties of the GNPs with different surface chemistry (Fig. S3b, ESI†).

3.2. Induction of cellular oxidative stress across two human cell lines by the GNPs with different physicochemical properties

Next, we examined the correlation of the physicochemical properties of nanoparticles with cellular oxidative stress in human cancer and normal cell lines from lungs and kidneys, where nanoparticles interact with cells when they get into circulation. Because high levels of oxidative stress may result in cell death, the correlation of the physicochemical properties

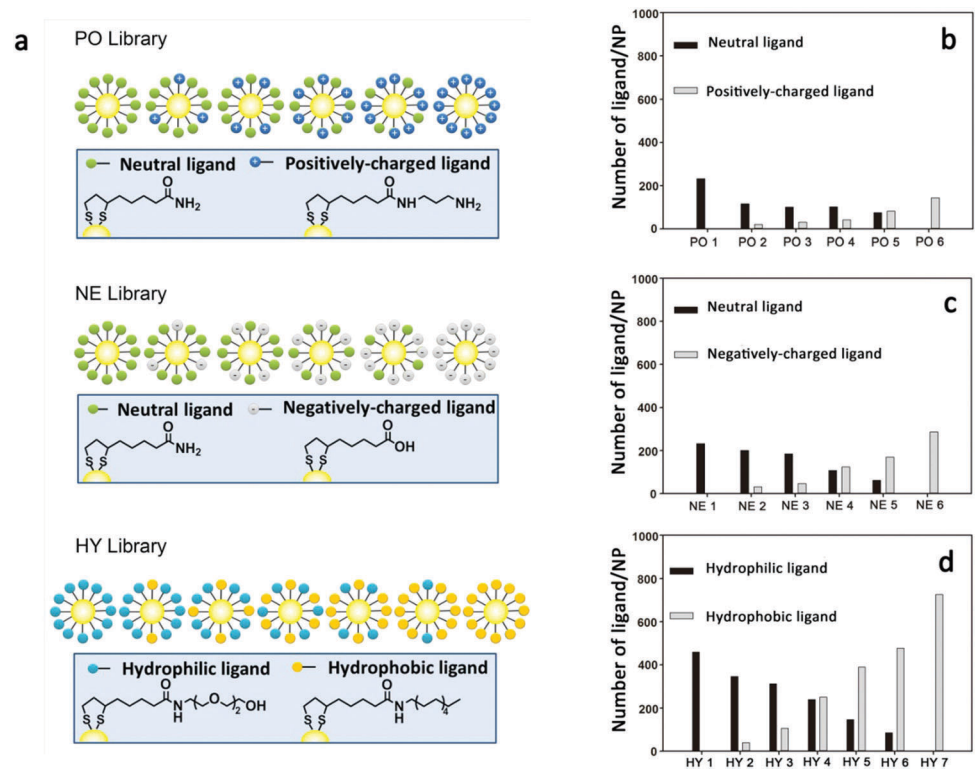

Fig. 1 The design and characterization of three GNP libraries with a gradient property change. (a) Three GNP libraries each exhibiting a gradient change in a specific physicochemical property, including positive charge (PO) density, negative charge (NE) density, and hydrophobicity (HY). The amount of different ligands on each GNP in (b) PO library, (c) NE library, and (d) HY library. Ligands on the GNPs were cleaved by I_2 treatment and the identity and the quantity of the surface ligands were analyzed by LC/MS as reported previously.[33]

of nanoparticles with cellular oxidative stress cannot be examined at such a stage. We first tested the cytotoxicity of the GNPs and selected 50 μg mL^{-1} as the GNP concentration at which the cell viability was more than 90% for all the GNPs (Fig. S4, ESI†). Heme oxygenase 1 (HO-1) is an enzyme that catalyzes the degradation of heme. Its expression is proportional to the cellular oxidative stress.[27] To investigate which physicochemical properties of nanoparticles have the propensity to induce cellular oxidative stress, we determined the expression levels of HO-1 by western blot (Fig. 2a) at a sublethal GNP concentration in the A549 cells. If the HO-1 expression level correlates with the gradient change of a specific nanoparticle property, that property can be identified as an inducer of oxidative stress. We then quantitatively determined the expression levels of HO-1 using ImageJ and our data showed that gradient changes in positive charge density and hydrophobicity were correlated with the HO-1 levels (Fig. 2b and c), while changes in negative charge density showed no correlation (Fig. 2b).

Besides the expression of HO-1, cellular H_2O_2 is also a key component of cellular oxidative stress. We then quantitatively determined the cellular H_2O_2 level induced by the GNPs with different physicochemical properties by the ROS-Glo™ H_2O_2 assay. The results obtained from the A549 and HEK293 cells (Fig. S5, ESI†) confirmed that the induction of cellular oxidative stress was affected by the hydrophobicity and positive charge density of the GNPs in multiple human cell lines.

Upon entering the human blood circulation system or organs, nanoparticles will adsorb proteins.[34] To test whether the oxidative stress induction was due to protein depletion on the nanoparticles in the cell culture medium, we compared the intracellular H_2O_2 levels induced by the GNPs in the cell culture medium with serum protein concentrations of 10% or 50%. The same trends of oxidative stress induction by the hydrophobicity and positive charge density of the GNPs were observed at both 10% and 50% serum protein concentrations (Fig. S6, ESI†). These results demonstrated that the induction of cellular oxidative stress was not caused by protein depletion.

3.3. Requirement of endocytosis for nanoparticle-induced oxidative stress generation

Nanoparticle-induced oxidative stress possibly resulted from the interactions between the nanoparticles and the cells during the cell binding and internalization process. To examine how the GNPs interact with the cells, we first examined the cellular uptake of the GNPs using TEM. The TEM images showed that hydrophobic HY 7 and positively charged PO 6 were significantly internalized by the cells in 24 h, while relative hydrophilic nanoparticle HY 1 and neutral nanoparticle PO 1 were internalized in much less amount (Fig. 3a). We then quantitatively determined the cellular uptake of the GNPs per cell using ICP-MS analysis and compared that with the cellular H_2O_2 level. Our results showed that the nanoparticle cellular uptake is correlated well with H_2O_2 levels (Fig. 3b and c) in the A549 cells. To establish a dependence of cellular oxidative stress on the cellular uptake of nanoparticles, an endocytosis inhibitor cytochalasin D (Cyto D) was used to inhibit the cellular uptake of PO 6 and HY 7. The Cyto D-induced reduction of cellular uptake of PO 6 and HY 7 caused a decrease in the H_2O_2 levels in the A549 cells in a concentration-dependent manner (Fig. 3d and e). In conclusion, the internalization of the hydrophobic or positively charged GNPs played an important role in generating the cellular oxidative stress.

3.4. Different mechanisms involved in the induction of oxidative stress by the hydrophobic and positively charged nanoparticles

Perturbations on mitochondria and NADPH oxidase are two of the known mechanisms of oxidative stress induction. We first employed a chemical–biological method to distinguish how the hydrophobic and positively charged nanoparticles caused oxidative stress. Apocynin (APO) and diphenyleneiodonium chloride (DPI) are inhibitors of NADPH oxidase while rotenone (ROT) is an inhibitor of mitochondrial respiratory chain complex-1.

We first investigated oxidative stress generation in the presence or absence of these inhibitors. APO and DPI suppressed the

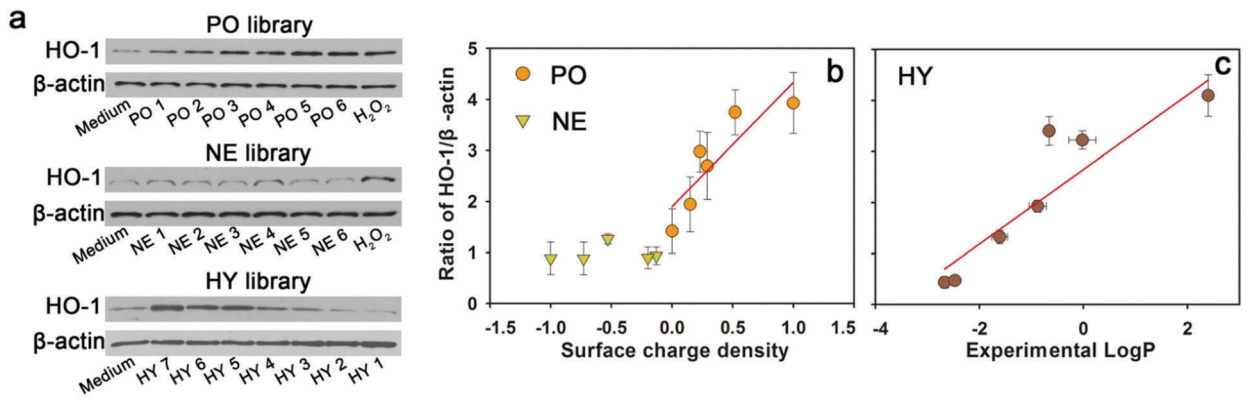

Fig. 2 Induction of oxidative stress by different GNP libraries. (a) Heme oxygenase 1 (HO-1) level in the A549 cells after incubation with the GNPs (50 μg mL^{-1}) from the three libraries. H_2O_2 (200 μM) was used as a positive control. β-Actin was used as a loading control. (b and c) HO-1/β-actin ratio in the A549 cells after incubation with the GNPs from the three libraries, as determined using the band density. The relationship between the HO-1 level and the physicochemical properties of nanoparticles is shown. Error bars indicate mean ± standard deviation (n = 3).

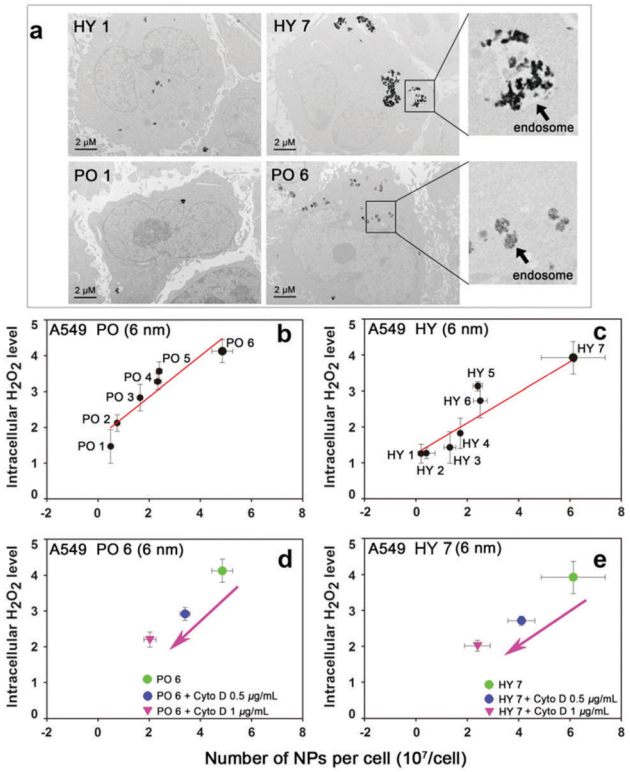

Fig. 3 The relationship between oxidative stress and cellular uptake of the GNPs from the PO and HY libraries. (a) TEM images of the A549 cells after incubation with the GNPs from the HY and PO libraries. (b and c) The correlation between the intracellular H_2O_2 level and cellular uptake of the GNPs. (d and e) The effect of Cyto D on the intracellular H_2O_2 and the cellular uptake of the GNPs.

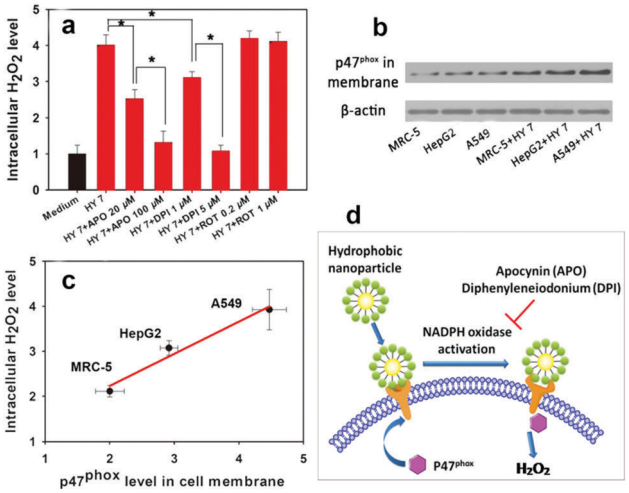

Fig. 4 Induction of hydrophobic nanoparticles oxidative stress through perturbing NADPH oxidase. (a) The intracellular H_2O_2 level in the A549 cells induced by HY 7 in the presence of apocynin (APO), diphenyleneiodonium chloride (DPI), or rotenone (ROT). The intracellular H_2O_2 level was determined by the ROS-Glo™ H_2O_2 assay. (b) The $p47^{phox}$ level in the cell membranes of the MRC-5, HepG2 and A549 cells before and after incubation with HY 7. The $p47^{phox}$ level in the cell membranes was determined by western blot. β-Actin was used as the loading control. (c) The relationship between the $p47^{phox}$ level in the cell membranes and the intracellular H_2O_2 level induced by HY 7 in different cell lines with various levels of NADPH oxidase. The band density in b was quantified using ImageJ. Error bars indicate mean ± standard deviation (n = 3). (d) Schematic illustration of the hydrophobic nanoparticles inducing the intracellular H_2O_2 level by perturbing NADPH oxidase.

intracellular H_2O_2 induction by HY 7 in an inhibitor concentration dependent manner (Fig. 4a), while ROT had little effect. These data indicated that the hydrophobic GNPs likely induced oxidative stress through NADPH oxidase perturbation. The activation of NADPH oxidase normally causes the translocation of its cytosolic subunits $P47^{phox}$ to the cell membrane.[35] Therefore, we next examined the $P47^{phox}$ level in the cell membrane by western blot (Fig. 4b). Cell lines MRC-5, HepG2, and A549 have different $P47^{phox}$ levels. MRC-5 has the lowest, while A549 has the highest $P47^{phox}$ levels. We therefore investigated whether the oxidative stress induction is correlated with NADPH oxidase activation by HY 7. We found that the intracellular H_2O_2 level was correlated with the $P47^{phox}$ level in the cell membranes in these cell lines in a NADPH oxidase-dependent manner (Fig. 4c). The above results demonstrated that the hydrophobic nanoparticles induced cellular oxidative stress mainly by perturbing NADPH oxidase (Fig. 4d).

Highly charged nanoparticles are expected to show very different interactions with cells compared to the hydrophobic nanoparticles, although both of them were heavily internalized by cells.[36] We observed that mitochondrial respiratory chain complex-1 inhibitor ROT suppressed the PO 6-induced intracellular H_2O_2 level in a dose-dependent manner, while APO and DPI had little effect (Fig. 5a). The surface positive charge density increases from PO 1 to PO 6. Nanoparticles PO 2, 4 and 6 induced a gradual increase in the levels of H_2O_2, and H_2O_2 generation was inhibited by ROT (Fig. S7, ESI†). These results indicated that the positively charged GNPs might induce oxidative stress through mitochondrial perturbation.

Since PI3K/Akt activation or an altered intracellular calcium concentration possibly regulate the cellular oxidative stress through mitochondria,[37] we first tested whether PO 6 induced H_2O_2 by activating the PI3K/Akt pathway. Our results showed that PO 6 did not activate the PI3K/Akt pathway (Fig. S8, ESI†). However, we found that the positively charged nanoparticles induced an increase in the intracellular calcium level. The enhanced calcium level was also correlated with the intracellular H_2O_2 level (Fig. 5b). The calcium chelating agent alleviated the intracellular H_2O_2 level induced by PO 6, suggesting that the influence of calcium ions was included in oxidative stress induction (Fig. S9a, ESI†). Nifedipine, a voltage-dependent calcium channel inhibitor, suppressed the intracellular calcium level in a dose dependent manner, and also decreased the intracellular H_2O_2 level (Fig. S9b, ESI†). Voltage-dependent calcium channels are a group of voltage-gated ion channels in cell membranes, which are sensitive to cell membrane potential.[38,39] Cell membrane depolarization activates voltage-dependent calcium channels, resulting in the translocation of calcium into cells. The opening of voltage-dependent calcium channels could be attributed to the membrane depolarization. This was then confirmed by the finding that PO 6 induced dose-dependent cell membrane depolarization (Fig. 5c). Taken together, these data demonstrated that the positively

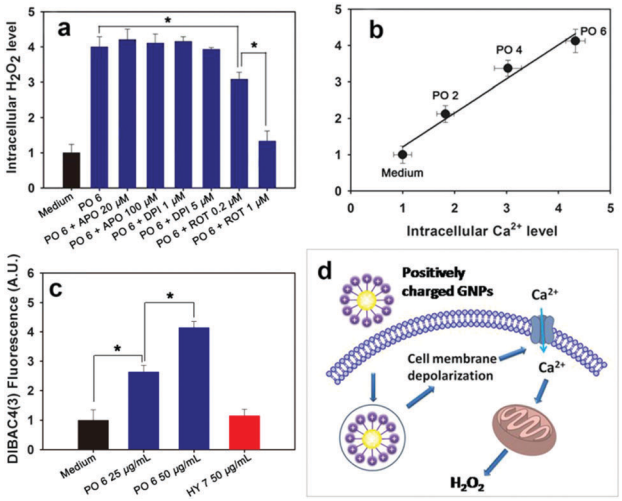

Fig. 5 Induction of positively charged GNPs oxidative stress through the mitochondria pathway. (a) The intracellular H_2O_2 level in the A549 cells induced by PO 6 in the presence of apocynin (APO), diphenyleneiodonium chloride (DPI), or rotenone (ROT). The intracellular H_2O_2 level was determined by the ROS-Glo™ H_2O_2 assay. (b) The correlation of the intracellular Ca^{2+} level and the intracellular H_2O_2 level in the A549 cells treated with the GNPs from the PO library. Intracellular Ca^{2+} levels were quantitatively determined by Fluo-3 AM. (c) Cell membrane potential perturbations by PO 6. Cell membrane potential was detected using $DIBAC_4(3)$. $^*P < 0.05$. Error bars indicate mean ± standard deviation (n = 3). (d) Schematic illustration of the positively charged nanoparticles inducing cell membrane depolarization and calcium channel opening, and stimulation of mitochondria to generate intracellular oxidative stress.

charged nanoparticles induced cell membrane depolarization and enhanced the cellular calcium concentration. The increase in the calcium concentration then stimulated the mitochondria to generate intracellular oxidative stress (Fig. 5d). Oxidative stress induced through different mechanisms may afford versatile strategies for the design of nanomedicines, such as biocompatible nanocarriers and cancer therapeutics.

3.5. Sensitization of the cancer cells to paclitaxel by oxidative stress induced by the positively charged and hydrophobic nanoparticles

The positively charged and hydrophobic nanoparticles induce cellular oxidative stress, which may sensitize the cancer cells to chemotherapeutics. To confirm this, we determined the EC_{50} of paclitaxel (PTX) in the presence or absence of the positively charged and hydrophobic GNPs in HeLa cells (Fig. 6). The concentration of the GNPs was 50 μg mL^{-1}, at which no cytotoxicity was observed for PO 6 and HY 7 (Fig. S10, ESI†). PO 6 and HY 7 enhanced the cytotoxicity of PTX by 200% compared with PTX alone (Fig. 6a). Meanwhile, a distinct increase of the intracellular H_2O_2 level was confirmed (Fig. 6b). To further investigate the role of oxidative stress in the sensitization of cancer cells, an ROS scavenger, *N*-acetyl-L-cysteine (NAC), was used with PO 6 and HY 7. NAC reduced the intracellular H_2O_2 level induced by PO 6 and HY 7 by 75% and caused a reduced cytotoxicity of PTX. Therefore, oxidative stress induced by the positively charged and hydrophobic nanoparticles

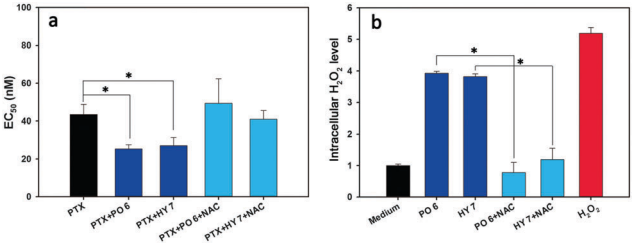

Fig. 6 Sensitization of cancer cells to PTX by oxidative stress induced by the positively charged and hydrophobic nanoparticles. (a) HeLa cells were treated with various concentrations of PTX (0.1 nM–10 μM) in the presence or absence of 50 μg mL^{-1} of PO 6, HY 7, and *N*-acetyl-L-cysteine (NAC, 10 mM) for 24 h. Cell viability was determined by the CellTiter-Glo® Luminescent cell viability assay. (b) HeLa cells were treated with 50 μg mL^{-1} of PO 6 or HY 7 in the presence or absence of NAC (10 mM) for 24 h. The intracellular H_2O_2 level was determined by the ROS-Glo™ H_2O_2 assay. Error bars indicate mean ± standard deviation (n = 3).

sensitizes the cancer cells to PTX. Both small molecules and biomolecules were reported to enhance the effects of chemotherapeutics by enhancing intracellular ROS levels.[8,9] Although nanoparticles were generally reported to be ROS inducers, synergistic effects in cancer treatment between nanoparticle-induced oxidative stress and chemotherapeutic drugs were rarely reported. Our findings that both positively charged and hydrophobic GNPs sensitized cancer cells to PTX through induction of oxidative stress provided the structural parameters for the design of future nanomedicine.

4. Conclusions

The understanding and appropriate manipulation of cellular oxidative stress are needed for both disease control and drug development. We have previously demonstrated that nanoparticles with certain modifications tuned cell functions through binding to receptors on cell membranes.[33,40–42] Employing nanoparticle libraries with a unique design, in this paper we revealed that the key nanoparticle properties, *e.g.*, hydrophobicity and positive charge, induced cellular oxidative stress which then sensitized the cancer cells to chemotherapeutic agents. Our findings that hydrophobic nanoparticles induce oxidative stress through NADPH oxidase perturbation while positively charged nanoparticles induce it through alteration of the mitochondria pathway further revealed the sophistication of cellular responsive machinery to nanoparticle perturbations. Our findings provide useful guidance for designing nano-theranostics with various purposes, such as designing novel biocompatible nanocarriers that induce no oxidative stress for diagnosis or nanomedicines that induce certain levels of oxidative stress to sensitize cancer cells to chemotherapy.

Conflicts of interest

There are no conflicts to declare.

Acknowledgements

This work was supported by the National Key Research and Development Program of China (2016YFA0203103), the National Natural Science Foundation of China (91543204 and 91643204), and the Strategic Priority Research Program of the Chinese Academy of Sciences (XDB14030401).

Notes and references

1 T. Finkel and N. J. Holbrook, *Nature*, 2000, **408**, 239–247.
2 M. Valko, D. Leibfritz, J. Moncol, M. T. Cronin, M. Mazur and J. Telser, *Int. J. Biochem. Cell Biol.*, 2007, **39**, 44–84.
3 H. Misonou, M. Morishima-Kawashima and Y. Ihara, *Biochemistry*, 2000, **39**, 6951–6959.
4 A. C. Maritim, R. A. Sanders and J. B. Watkins, *J. Biochem. Mol. Toxicol.*, 2003, **17**, 24–38.
5 D. Harrison, K. K. Griendling, U. Landmesser, B. Hornig and H. Drexler, *Am. J. Cardiol.*, 2003, **91**, 7–11.
6 M. Valko, C. Rhodes, J. Moncol, M. Izakovic and M. Mazur, *Chem. – Biol. Interact.*, 2006, **160**, 1–40.
7 T. Ozben, *J. Pharm. Sci.*, 2007, **96**, 2181–2196.
8 X. Li, X. Lu, H. Xu, Z. Zhu, H. Yin, X. Qian, R. Li, X. Jiang and B. Liu, *Mol. Pharmaceutics*, 2011, **9**, 222–229.
9 Y. Sawayama, Y. Miyazaki, K. Ando, K. Horio, C. Tsutsumi, D. Imanishi, H. Tsushima, Y. Imaizumi, T. Hata, T. Fukushima, S. Yoshida, Y. Onimaru, M. Iwanaga, J. Taguchi, K. Kuriyama and M. Tomonaga, *Leukemia*, 2008, **22**, 956–964.
10 M. F. De Volder, S. H. Tawfick, R. H. Baughman and A. J. Hart, *Science*, 2013, **339**, 535–539.
11 P. Avouris, Z. Chen and V. Perebeinos, *Nat. Nanotechnol.*, 2007, **2**, 605–615.
12 P. Lin, L. Hu and X. Fang, *Adv. Funct. Mater.*, 2014, **24**, 2591–2610.
13 A. S. Aricò, P. Bruce, B. Scrosati, J. Tarascon and W. V. Schalkwijk, *Nat. Mater.*, 2005, **4**, 366–377.
14 D. Peer, J. M. Karp, S. Hong, O. C. Farokhzad, R. Margalit and R. Langer, *Nat. Nanotechnol.*, 2007, **2**, 751–760.
15 G. Chen, I. Roy, C. Yang and P. N. Prasad, *Chem. Rev.*, 2016, **116**, 2826–2885.
16 L. A. Lane, X. Qian and S. Nie, *Chem. Rev.*, 2015, **115**, 10489–10529.
17 A. Weir, P. Westerhoff, L. Fabricius, K. Hristovski and N. bon Goetz, *Environ. Sci. Technol.*, 2012, **46**, 2242–2250.
18 J. Weiss, P. Takhistov and D. J. Mcclements, *J. Food Sci.*, 2006, **71**, R107–R116.
19 Y. J. Kim, M. Yu, H. O. Park and S. I. Yang, *Mol. Cell. Toxicol.*, 2010, **6**, 336–343.
20 T. Xia, M. Kovochich, M. Liong, L. Mädler, B. Gilbert, H. Shi, J. I. Yeh, J. I. Zink and A. E. Nel, *ACS Nano*, 2008, **2**, 2121–2134.
21 M. S. Wason, J. Colon, S. Das, S. Seal, J. Turkson, J. Zhao and C. H. Baker, *Nanomedicine*, 2013, **9**, 558–569.
22 H. Zhang, Z. Ji, T. Xia, H. Meng, C. Low-Kam, R. Liu, S. Pokhrel, S. Lin, X. Wang, Y.-P. Liao, M. Wang, L. Li, R. Rallo, R. Damoiseaux, D. Telesca, L. Mädler, Y. Cohen, J. I. Zink and A. E. Nel, *ACS Nano*, 2012, **6**, 4349–4368.
23 S. George, T. Xia, R. Rallo, Y. Zhao, Z. Ji, S. Lin, X. Wang, H. Zhang, B. France, D. Schoenfeld, R. Damoiseaux, R. Liu, S. Lin, K. A. Bradley, Y. Cohen and A. E. Nel, *ACS Nano*, 2011, **5**, 1805–1817.
24 C. Carlson, S. M. Hussain, A. M. Schrand, L. K. Braydichstolle, K. L. Hess, R. L. Jones and J. J. Schlager, *J. Phys. Chem. B*, 2008, **112**, 13608–13619.
25 H. Persson, C. Købler, K. Mølhave, L. Samuelson, J. O. Tegenfeldt, S. Oredsson and C. N. Prinz, *Small*, 2013, **9**, 4006–4016.
26 A. Chompoosor, K. Saha, P. S. Ghosh, D. J. Macarthy, O. R. Miranda, Z. J. Zhu, K. F. Arcaro and V. M. Rotello, *Small*, 2010, **6**, 2246–2249.
27 T. Xia, M. Kovochich, J. Brant, M. Hotze, J. Sempf, T. Oberley, C. Sioutas, J. I. Yeh, M. R. Wiesner and A. E. Nel, *Nano Lett.*, 2006, **6**, 1794–1807.
28 S. Li, S. Zhai, Y. Liu, H. Zhou, J. Wu, Q. Jiao, B. Zhang, H. Zhu and B. Yan, *Biomaterials*, 2015, **52**, 312–317.
29 X. Hu, A. Sun, W. Kang and Q. Zhou, *Environ. Int.*, 2017, **102**, 177–189.
30 X. Zhang, Q. Zhou, W. Zou and X. Hu, *Environ. Sci. Technol.*, 2017, **51**, 7861–7871.
31 L. Mu, Y. Gao and X. Hu, *Biomaterials*, 2015, **52**, 301–311.
32 G. Su, X. Zhou, H. Zhou, Y. Li, X. Zhang, Y. Liu, D. Cao and B. Yan, *ACS Appl. Mater. Interfaces*, 2016, **8**, 30037–30047.
33 H. Zhou, P. Jiao, L. Yang, X. Li and B. Yan, *J. Am. Chem. Soc.*, 2010, **133**, 680–682.
34 B. D. Chithrani, A. A. Ghazani and W. C. W. Chan, *Nano Lett.*, 2006, **6**, 662–668.
35 K. Bedard and K.-H. Krause, *Physiol. Rev.*, 2007, **87**, 245–313.
36 X. Tao, S. Jin, D. Wu, K. Ling, L. Yuan, P. Lin, Y. Xie and X. Yang, *Nanomaterials*, 2016, **6**, 2.
37 L. A. Sena and N. S. Chandel, *Mol. Cell*, 2012, **48**, 158–167.
38 L. Lacinová, *Gen. Physiol. Biophys.*, 2005, **24**, 1–78.
39 N. Klugbauer, *Rev. Physiol., Biochem. Pharmacol.*, 1999, **139**, 33–87.
40 Y. Zhang, Q. Mu, H. Zhou, K. Vrijens, M. Roussel, G. Jiang and B. Yan, *Cell Death Dis.*, 2012, **3**, e308.
41 N. Gao, Q. Zhang, Q. Mu, Y. Bai, L. Li, H. Zhou, E. R. Butch, T. B. Powell, S. E. Snyder, G. Jiang and B. Yan, *ACS Nano*, 2011, **5**, 4581–4591.
42 P. Jiao, H. Zhou, M. Otto, Q. Mu, L. Li, G. Su, Y. Zhang, E. R. Butch, S. E. Snyder, G. Jiang and B. Yan, *J. Am. Chem. Soc.*, 2011, **133**, 13918–13921.